COMPUTING EIGENFUNCTIONS ON THE KOCH SNOWFLAKE: A NEW GRID AND SYMMETRY.

JOHN M. NEUBERGER, NÁNDOR SIEBEN, AND JAMES W. SWIFT

ABSTRACT. In this paper we numerically solve the eigenvalue problem $\Delta u+\lambda u = 0$ on the fractal region defined by the Koch Snowflake, with zero-Dirichlet or zero-Neumann boundary conditions. The Laplacian with boundary conditions is approximated by a large symmetric matrix. The eigenvalues and eigenvectors of this matrix are computed by ARPACK. We impose the boundary conditions in a way that gives improved accuracy over the previous computations of Lapidus, Neuberger, Renka & Griffith. We extrapolate the results for grid spacing h to the limit $h \to 0$ in order to estimate eigenvalues of the Laplacian and compare our results to those of Lapdus et al. We analyze the symmetry of the region to explain the multiplicity-two eigenvalues, and present a canonical choice of the two eigenfunctions that span each two-dimensional eigenspace.

1. INTRODUCTION.

In this paper we approximate solutions to the two eigenvalue problems

$$\begin{aligned} \Delta u + \lambda u &= 0 \quad \text{in } \Omega & \qquad \Delta u + \lambda u &= 0 \quad \text{in } \Omega \\ u &= 0 \quad \text{on } \partial\Omega \text{ (D)} & \qquad \frac{\partial u}{\partial \eta} &= 0 \quad \text{on } \partial\Omega \text{ (N)}, \end{aligned} \tag{1.1}$$

where Δ is the Laplacian operator, and $\Omega \subset \mathbb{R}^2$ is the (open) region whose boundary $\partial\Omega$ is the Koch snowflake. For convenience, we refer to Ω as the *Koch snowflake region*. The boundary conditions are zero-Dirichlet, or zero-Neumann, respectively.

These boundary value problems must be interpreted in the variational sense (see [Lapidus, 1991]) but we avoid the subtleties of functional analysis by discretizing the problem. We use a triangular grid of points to approximate the snowflake region. Then, we identify $u : \Omega \to \mathbb{R}$ with $u \in \mathbb{R}^N$, where N is the number of grid points in Ω. That is,

$$u(x_i) \approx u_i$$

at grid points $x_i \in \mathbb{R}^2$, $i \in \{1, 2, 3, \ldots, N\}$. The *discretized Laplacian* is the symmetric matrix L, with the property

$$(-\Delta u)(x_i) \approx (Lu)_i = \sum_{j=1}^{N} L_{ij} u_j.$$

Of course, a specific grid and a scheme for enforcing the boundary conditions are needed to define L. This is described in Section 2. Then, the eigenvalues and eigenfunctions of L approximate the eigenvalues and eigenfunctions defined by (1.1). The eigenvalues and eigenvectors of L are our approximations of the eigenvalues $0 \le \lambda_1 < \lambda_2 \le \lambda_3 \le \cdots \le \lambda_k \cdots \to \infty$ and the corresponding eigenfunctions $\{\psi_k\}_{k=1}^{\infty}$ of the negative Laplacian $-\Delta$.

The Koch snowflake is a well known fractal, with Hausdorff dimension $\log_3 4$. Following Lapidus, Neuberger, Renka, and Griffith [Lapidus et al., 1996], we take our snowflake to be inscribed in a circle of radius $\frac{\sqrt{3}}{3}$ centered about the origin. With this choice, the polygonal approximations used

2000 *Mathematics Subject Classification.* 20C35, 35P10, 65N25.

Key words and phrases. Snowflake, symmetry, eigenvalue problem.

Partially supported by NSF Grant DMS-0074326.

October 6, 2010.

in the fractal construction have side length that are powers of 1/3. In [Lapidus et al., 1996], a triangular grid with spacing $h = h_{\rm LNR}(\ell) = 1/3^\ell$ was used to approximate the eigenfunctions. Here ℓ is a positive integer indicating the mesh size and the *level* of polygonal approximation to the fractal boundary. With this choice of h, there are $N_{\rm NLR}(\ell) = 1 + (4 \cdot 9^\ell - 9 \cdot 4^\ell)/5$ grid points in Ω, as well as $3 \cdot 4^\ell$ grid points on $\partial\Omega$ (see Table 1). The zero-Dirichlet boundary conditions are imposed by setting $u_i = 0$ at the grid points on the boundary.

We used a different triangular grid. We found *more accurate* results with a *larger* h by choosing the grid spacing to be $h = h_{\rm NSS}(\ell) = 2/3^\ell$ and placing the boundary between grid points. This yields $N = N_{\rm NSS}(\ell) = (9^\ell - 4^\ell)/5$ grid points in the snowflake region Ω. No grid points are on $\partial\Omega$ with our choice. We use *ghost points*, which are outside the region, to enforce the boundary conditions, as described in Section 2. To compare our results with those of [Lapidus et al., 1996] we will use $\lambda_k^{(\ell)}$ to denote the $k^{\rm th}$ eigenvalue of L at level ℓ with our method, and $\mu_k^{(\ell)}$ to denote the eigenvalues published in [Lapidus et al., 1996].

ℓ	1	2	3	4	5	6
$N_{\rm NSS}(\ell)$	1	13	133	1261	11605	105469
$N_{\rm LNR}(\ell)$	1	37	469	4789	45397	417781

TABLE 1. The number of interior grid points with $h = h_{\rm NSS}(\ell) = 2/3^\ell$ (the current work), and with $h = h_{\rm LNR}(\ell) = 1/3^\ell$ as in [Lapidus et al., 1996]. Note that our new grid has approximately 75% fewer grid points at the same ℓ, when ℓ is large. The region Ω is open and the larger values of N published in [Lapidus et al., 1996] includes the grid points on the boundary.

A different approach, avoiding triangular grids altogether, can be found in the unpublished thesis [Banjai, 2003]. This work uses the conformal mappings found in [Banjai & Trefethen, 2003].

In [Neuberger and Swift, 2001], the Gradient Newton Galerkin Algorithm (GNGA) was developed to investigate existence, multiplicity, nodal structure, bifurcation, and symmetry of problems of the form (5.1). (This PDE is found in the concluding section.) The GNGA requires as input an orthonormal basis of a sufficiently large subspace consisting of eigenfunctions of the Laplacian. Since our eventual application concerns solving the nonlinear equation (5.1) on the region Ω with fractal boundary, we face the considerable challenge of first obtaining eigenfunctions (solutions to the linear problem (1.1)) numerically. In [Lapidus et al., 1996], this was done using essentially the inverse power method with deflation on a triangular grid. They used approximating boundary polygons with vertices at grid points.

Using our new grid, we improve upon their results and are substantially successful in obtaining a basis of such functions for a sufficiently large subspace for our future nonlinear needs. We use the sophisticated numerical package ARPACK instead of deflation. This software is based upon an algorithmic variant of the Arnoldi process called the Implicitly Restarted Arnoldi Method (see [Lehoucq et al., 1998]) and is ideally suited for finding the eigen-pairs of the large sparse matrices associated with the discretization L of the Laplacian. It is easily implemented, requiring only a user-provided subroutine giving the action of the linear map. One of our innovations in investigating the snowflake is taking the boundary to lie between grid points and using ghost points just outside Ω when approximating the Laplacian at interior points closest to the boundary. This results in better approximations of true eigenvalues using fewer interior grid points than achieved by [Lapidus et al., 1996] using the standard grid method of enforcing the boundary condition. We support this claim by comparing our results via curve fitting data points to predict the true values.

In Section 2, we describe in more detail the triangular grid and the accompanying second difference scheme for approximating the Laplacian, as well as the ARPACK implementation using this information to generate the basis of eigenfunctions. In Section 3, we compare our numerical

eigenvalue approximations to those obtained in [Lapidus et al., 1996]. In particular, we perform Richardson extrapolations on both data sets. In Section 4, we apply representation theory to determine the 8 possible symmetries that eigenfunctions (and approximating eigenvectors) can have, given the $\mathbb{D}_6$ symmetry of the region Ω and the approximating grids. We consider this rigorous treatment of symmetry to be a key contribution of this paper. This information is used for numerical post-processing to find symmetric "canonical" representatives for multiple eigenvalues. This catalog of the symmetries of basis elements will be used in an essential way in our subsequent nonlinear bifurcation studies. Section 4 also contains graphics depicting a selection of approximating eigenvectors to both problems in (1.1). Section 5 gives a brief indication of how our new grid can be used when implementing GNGA on related nonlinear problems (see [Neuberger, Sieben, and Swift II]). Also, we discuss how the known symmetries can be exploited to reduce the number of integrations required by that scheme.

2. Ghost Points and ARPACK.

In approximating the Laplacian for functions defined on Ω, we developed the grid technique depicted in Figure 1. As in [Lapidus et al., 1996], at interior points with interior point neighbors one sees that the standard second-differencing scheme when applied to a triangular grid leads to the approximation

$$-\Delta u(x) \approx \frac{2}{3h^2}\left(6u(x) - \sum\{\text{6 neighbor values of } u\}\right).$$

Our scheme differs, however, when computing approximations at interior grid points with neighbors that lie *outside* the boundary. In [Lapidus et al., 1996] the value of zero at boundary points (which lie on their grid) is used to enforce the zero-Dirichlet boundary condition. When we approximate the Laplacian at a point x_i near the boundary, we set $u = -u(x_i)$ at ghost points which are neighbors of x_i. Specifically, for the level $\ell = 2$ example found in Figure 1 and with the understanding that $u_i \approx u(x_i)$, we have

$$-\Delta u(x_1) \approx \frac{2}{3h^2}(6u_1 - (u_2 + u_3 + u_4 + u_5 + u_6 + u_7)),$$

$$-\Delta u(x_2) \approx \frac{2}{3h^2}(6u_2 - ((-u_2) + u_1 + u_3 + u_7 + u_8 + u_9)) = \frac{2}{3h^2}(7u_2 - (u_1 + u_3 + u_7 + u_8 + u_9)),$$

$$-\Delta u(x_9) \approx \frac{2}{3h^2}(6u_9 - ((-u_9) + (-u_9) + (-u_9) + (-u_9) + u_2 + u_3)) = \frac{2}{3h^2}(10u_9 - (u_2 + u_3)).$$

In the first line, there are no ghost points used because all the neighbors of x_1 are interior points. In the approximation at x_2, $(-u_2)$ represents the value of u at the ghost point g_1, as labelled in Figure 1. In the last line, $(-u_9)$ represents the value of u at $g_1, \ldots, g_4$. Note that the value of u at g_1 is different in the calculation at x_2 and x_9. An alternative way of imposing the boundary conditions is to set $u(g_1)$ to be the average of u_2, u_8, and u_9. We did experiments with this alternative method, but the results were not as accurate as the method we have described.

Our method of imposing the zero-Dirichlet boundary conditions can be summarized as

$$-\Delta u(x) \approx \frac{2}{3h^2}((12 - (\text{number of interior neighbors}))u(x) - \sum\{\text{interior neighbor values of } u\}).$$

The zero-Neumann boundary condition can be easily applied as well. Indeed, one has the only slightly different formula (which agrees away from the boundary)

$$-\Delta u(x) \approx \frac{2}{3h^2}((\text{number of interior neighbors})u(x) - \sum\{\text{interior neighbor values of } u\}).$$

To enforce the Neumann instead of the Dirichlet condition, we only need to change 3 characters of our ARPACK code. Specifically, one deletes the "12−" found in the zero-Dirichlet formulae above.

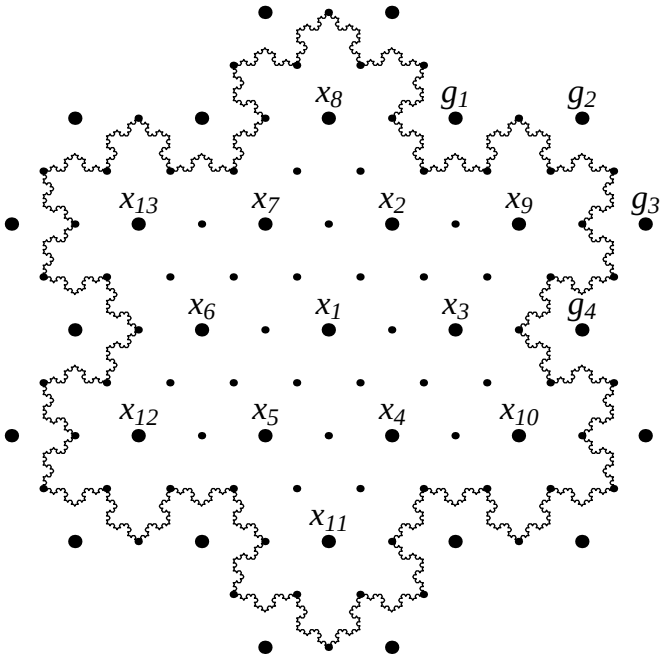

FIGURE 1. The Koch snowflake $\partial\Omega$ with $N_{\rm NSS}(2) = 13$ labelled grid points $\{x_i\}_{i=1}^{13}$ at level $\ell = 2$. The grid used by [Lapidus et al., 1996] consists of the $N_{\rm LNR}(2) = 37$ large and small points inside the snowflake, along with 48 small points on $\partial\Omega$. The points outside of the snowflake, some labelled g_i, are ghost points we use to enforce the boundary conditions. For example, $u(g_2) = -u(x_9)$ for Dirichlet boundary conditions and $u(g_2) = u(x_9)$ for Neumann boundary conditions. On the other hand, u takes on different values at g_1 when the Laplacian is evaluated at x_2, x_8, or x_9.

The user-provided ARPACK subroutine takes as input a vector $v \in \mathbb{R}^N$ and outputs $w \in \mathbb{R}^N$ with $w = Lv$ for the $N \times N$ matrix L approximating the discretized negative Laplacian, where for convenience we use N to denote $N_{\rm NSS}(\ell)$. This procedure is easily coded once an $N \times 6$ dimensional array t with neighbor information is populated. In the pseudocode in Figure 2, $t(i,j) \in \{0, 1, 2, \ldots, N\}$ is the index of the $j^{\rm th}$ neighbor of the grid point x_i, $j = 1, \ldots, 6$. If $t(i,j) = 0$ for some j, then the $i^{\rm th}$ interior point is near the boundary and has less than 6 interior point neighbors. We let $k_i \in \{2, 4, 5, 6\}$ denote the number of interior point neighbors of grid point x_i.

```
Loop for i = 1,...,N
 1. Set
      w(i) = { (12 - k_i) * v(i)   for Dirichlet boundary conditions, or
             {       k_i * v(i)   for Neumann
 2. Loop for j = 1,...,6
      a. Find index p = t(i,j) of j^th neighbor
      b. If p ≠ 0 then subtract neighbor value:  w(i) = w(i) - v(p)
 3. Multiply by h factor:  w(i) = 2 * w(i)/(3.0 * h * h)
```

FIGURE 2. Pseudo code for user-provided subroutine encoding the linear map $v \mapsto w = Lv$.

The neighbor file is generated using the `set` and `vector` data structures and the binary search algorithm of the Standard Template Library in `C++`. In the first step we find the integer coordinates

of the grid points in the basis $\{(1,0),(\frac{1}{2},\frac{\sqrt{3}}{2})\}$. The procedure uses simple loops to find the coordinates of the grid points inside a large triangle and then calls itself recursively on three smaller triangles placed on the three sides of the original triangle, until the desired level is reached. To avoid duplication of grid points the coordinates are collected in a `set` data structure. In the second step, we copy the coordinates into a `vector` data structure and use binary searches to find the indices of the six possible neighbors of each grid point. In the last step, we compute the Cartesian coordinates of the grid points and write them into a file together with the indices of the neighbors.

3. Numerical Results

In this section we present our experimental results. Our best approximations λ_k^{R} for the eigenvalues are obtained by performing Richardson extrapolation. Specifically, we find the y-intercepts of the Lagrange polynomials fitting the points $\{(h_{\mathrm{NSS}}(\ell),\lambda_k(\ell))\}_{\ell=4}^{6}$. We also compute Richardson extrapolations μ_k^{R} using the data published in [Lapidus et al., 1996]. In Table 2 we list the level 6 and Richardson approximations of the first ten and the 100^{th} eigenvalues.

k	NSS $\lambda_k(6)$	NSS λ_k^{R}	LNR $\mu_k(6)$	LNR μ_k^{R}
1	39.353	39.349	39.390	39.352
2	97.446	97.438	97.537	97.438
3	97.446	97.438	97.537	97.438
4	165.417	165.409	165.622	165.478
5	165.417	165.409	165.622	165.478
6	190.381	190.373	190.571	190.365
7	208.622	208.617	208.837	208.59
8	272.415	272.413	272.755	272.480
9	272.415	272.413	272.755	272.480
10	312.348	312.358	312.645	312.351
100	2322.129	2324.925		

Table 2. The first ten and the 100^{th} eigenvalues to the Dirichlet problem. NSS denotes our new grid, while LNR denotes the grid in [Lapidus et al., 1996]. Provided are the level $\ell = 6$ approximations, where the NSS scheme uses $N_{\mathrm{NSS}}(6) = 105469$ grid points and the LNR method uses $N_{\mathrm{LNR}}(6) = 417781$ interior grid points. The symbols λ_k^{R} and μ_k^{R} denote the the Richardson extrapolation values for λ_k using levels $\ell \in \{4,5,6\}$. Blank entries correspond to no data available for comparison.

We computed the relative differences $\left(\lambda_k(6)-\lambda_k^{\mathrm{R}}\right)/\lambda_k^{\mathrm{R}}$ and $\left(\mu_k(6)-\mu_k^{\mathrm{R}}\right)/\mu_k^{\mathrm{R}}$ for $k \in \{1,\ldots,10\}$. The relative differences of the λ values ranged from 10^{-5} to 10^{-4}, while the relative differences of the μ values are all on the order of 10^{-3}. The absolute differences between the Richardson extrapolations λ_k^{R} and μ_k^{R} ranged from 10^{-4} to $7\cdot 10^{-2}$. Note that even for $k = 100$ we have $\left(\lambda_{100}(6)-\lambda_{100}^{\mathrm{R}}\right)/\lambda_{100}^{\mathrm{R}} \approx -1.203\cdot 10^{-3}$.

In Figures 3 and 4 we visually compare the Richardson extrapolations for λ_1 and λ_{10}. We can see that although the extrapolated values are nearly identical, our approximations are much closer to the common extrapolated values using a lot fewer grid points. This is a key issue for us since in [Neuberger, Sieben, and Swift II] we will require accurate eigenvectors and eigenvalues using as few grid points as possible. We cannot use the extrapolated eigenvalues, since although they are more accurate approximations of eigenvalues of $-\Delta$, they are not eigenvalues of L corresponding to eigenvectors of L at any given level.

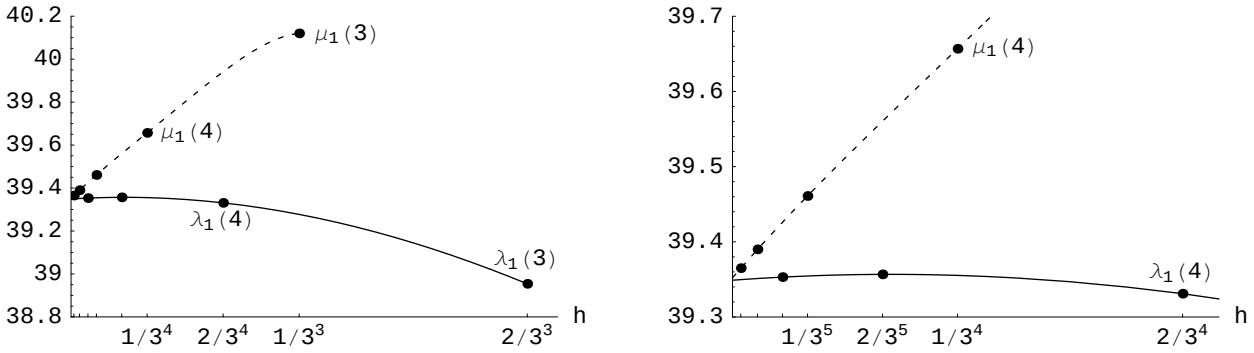

FIGURE 3. Two views of the Richardson extrapolations for λ_1. The solid line is the graph of the Lagrange polynomial fitting our data for $\ell \in \{3,4,5,6\}$. The dashed line fits the $\ell \in \{3,4,5,6\}$ data of [Lapidus et al., 1996] together with the unpublished level $\ell = 7$ eigenvalue approximation obtained via private communication from Robert Renka.

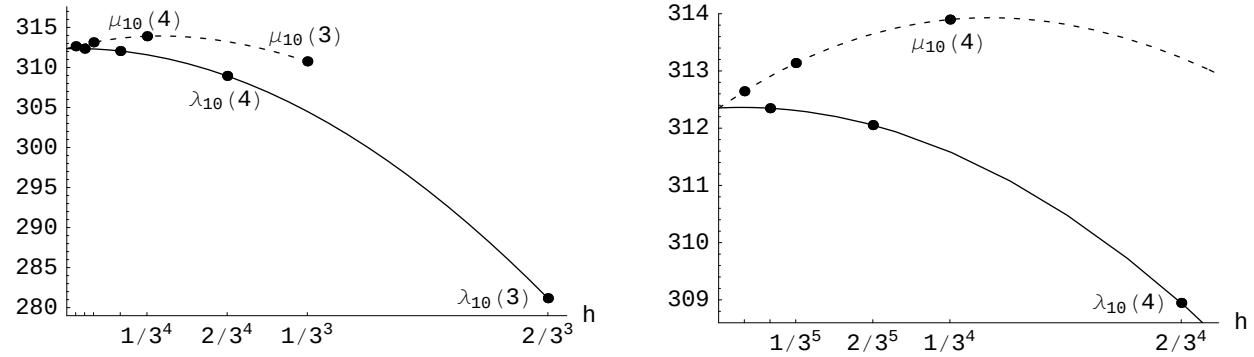

FIGURE 4. Two views of the Richardson Extrapolations for λ_{10}. As in Figure 3, the solid lines correspond to our data and the dashed lines to the data in [Lapidus et al., 1996].

Our results for the Neumann boundary conditions are shown in Table 3. Based on private communication we know that our approximate eigenvalues are very close to the unpublished numbers obtained by Lapidus et al. A careful comparison of the two grid schemes is not possible at this time, since we do not have all of their data. We found that the Lagrange polynomial of our Neumann data approaches $h = 0$ linearly, similar to the curves of [Lapidus et al., 1996] in Figures 3 and 4. This led us to consider an alternate scheme for enforcing boundary conditions. As noted in Figure 1, u is multi-valued at certain ghost points. We tried using a single average value at these ghost points, but the slope of the Lagrange polynomial at 0 was larger, so that the eigenvalues at a given level were farther from the extrapolated value. It is an area for future research to understand why the ghost points work so well. All we can now assert is that our method clearly out-performs that found in [Lapidus et al., 1996] for the zero-Dirichlet eigenvalue problem on the snowflake region. The ghost points can be used in general regions, and it would be interesting to determine the optimal method for enforcing boundary conditions on general regions.

We produced contour plots of the eigenfunctions. An example is shown in Figure 5. These contour plots were produced by a Mathematica notebook that reads in the u vector and outputs a postscript file. The level of the grid approximation is computed from the length of the u vector. All of the contour plots shown in this paper use $\ell = 5$ data for which the u vector has length $N_{\mathrm{NSS}}(5) = 11605$.

k	$\lambda_k(6)$	λ_k^{R}	$(\lambda_k(6)-\lambda_k^{\mathrm{R}})/\lambda_k^{\mathrm{R}}$
1	0.0000	0.0000	NA
2	11.9105	11.8424	0.0057
3	11.9105	11.8424	0.0057
4	23.1770	23.0466	0.0057
5	23.1770	23.0466	0.0057
6	27.5770	27.4261	0.0055
7	52.4164	52.2105	0.0039
8	85.8449	85.5521	0.0034
9	85.8449	85.5521	0.0034
10	112.7801	112.0200	0.0068
100	1295.4431	1271.1900	0.0191

TABLE 3. The first 10 and 100^{th} eigenvalues for the Neumann problem. We have included the level $\ell = 6$ approximations, the Richardson extrapolations using $\ell \in \{4, 5, 6\}$, and the relative differences of the two. All results use our new grid. The Neumann eigenvalues obtained by Lapidus et al. have not been published.

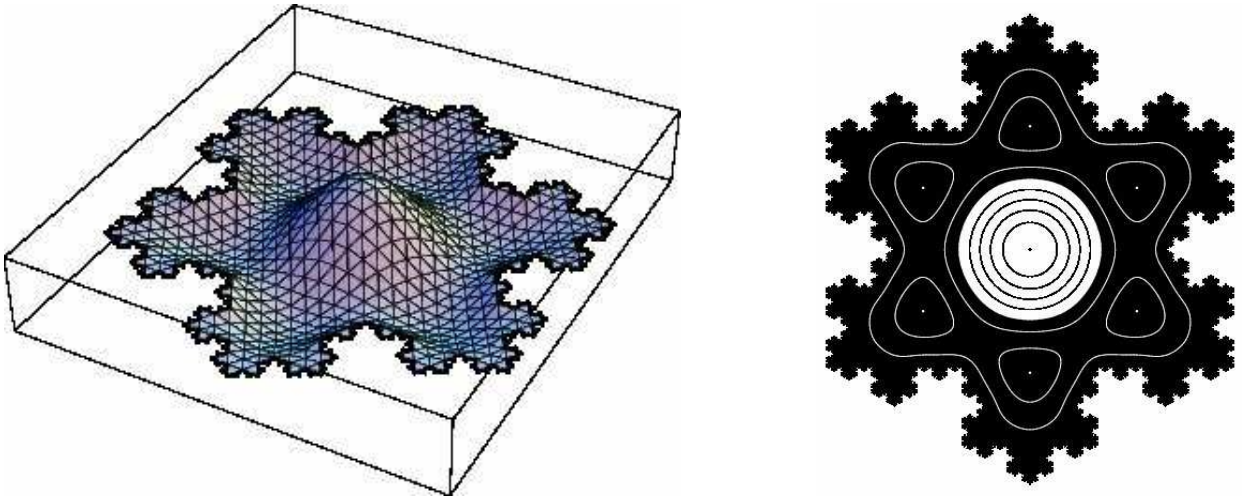

FIGURE 5. The graph, and a contour plot, of the sixth eigenfunction, ψ_6, with Dirichlet boundary conditions. The graph uses 469 grid points to triangulate the snowflake region. The contour plot shows our level $\ell = 5$ data with the new grid, as described in the text. The white and black regions in the contour plot represent positive and negative values of ψ_6. The contours are equally spaced, and the dots represent local extrema of ψ_6.

The local extrema of u are calculated in two steps. First the extreme values of u_i are calculated. Then, a quadratic fit to this data point and its six neighbors is performed. A dot is then drawn at the extremum of the quadratic function. This extra effort, compared to drawing a dot at the grid point, has a noticeable effect even at level 5. After the extrema are found, the u values of the contours are computed using a heuristic that gives fewer levels as the number of extrema increases.

The black regions are then drawn by subdividing the snowflake region into the triangles defined by the grid points. If $u < 0$ at all three vertices of a triangle then the triangle is filled with black. If $u < 0$ at some vertices of the triangle and $u > 0$ at others, then a linear interpolation is used to estimate the region where $u < 0$ within the triangle. The contours are also produced using linear

interpolation within the triangles: If the value of u on the vertices spans a contour value, then a short line segment inside the triangle is drawn based on the linear fit.

Several details of the implementation of the contour plotting have been left out. For example the region outside of the triangulation of grid points, but inside the snowflake boundary, is shaded by a different technique.

4. Symmetry and the Canonical Basis.

Some of the eigenvalues of the Laplacian on the snowflake, (1.1), have multiplicity one, and some have multiplicity two. In this section we quote well-known results in group representation theory to explain the observed multiplicity. We also describe a *canonical* way to choose two eigenvectors to span the two-dimensional eigenspaces. Details of group representation theory can be found in [Tinkham, 1964], [Sternberg, 1994] and [Scott, 1964].

Assume that G is a finite group. A *linear representation* of G is a homomorphism $\alpha : G \to GL(U)$ where $GL(U)$ is the group of invertible linear operators on the vector space $U = \mathbb{R}^N$ or $\mathbb{C}^N$. The vector space U is called the *representation space* of the linear representation. If B is a basis for U and $T \in GL(U)$ then we write $[T]_B$ for the matrix of T in the basis B or simply $[T]$ if B is the standard basis. We call the map $g \mapsto [\alpha(g)]$ a *matrix representation*. Two representations $\alpha, \beta : G \to H$ are *equivalent*, and we write $\alpha \sim \beta$, if there is an $h \in H$ such that $\beta(g) = h^{-1}\alpha(g)h$ for all $g \in G$.

Let $\alpha : G \to GL(U)$ be a linear representation. If $g \in G$ then $\alpha(g) : U \to U$ is a linear operator; for convenience we sometimes use the notation $\alpha_g = \alpha(g)$. The linear representation α induces a *group action* $G \times U \to U$. We often write $g \cdot u$ in place of $\alpha_g(u)$ when the representation α is understood.

A subspace W of U is called an *invariant subspace* of α if $\alpha_g(W) \subseteq W$ for all $g \in G$. The representation α is called *irreducible* if α has no proper invariant subspaces. The property of complete reducibility, also known as Maschke's theorem, says that there are α-invariant subspaces $U_1, \ldots, U_k$ such that $U = U_1 \oplus \cdots \oplus U_k$ and $\gamma^{(n)} := \alpha|_{U_n}$ is irreducible for each $n \in \{1, \ldots, k\}$. If B_n is a basis for U_n and $B = \cup_n B_n$ then the matrix of α_g in the basis B is block diagonal for all $g \in G$, that is

$$[\alpha_g]_B = \bigoplus_{n=1}^{k} [\gamma^{(n)}(g)]_{B_n}.$$

Let $\Gamma^{(i)}$, $i \in \{1, \ldots, q\}$ be an element from each of the q equivalence classes of irreducible representations of G. Suppose we have a complete decomposition of the representation α into irreducible representations $\gamma^{(n)}$. For each i there is an α-invariant subspace

$$V^{(i)} = \bigoplus \{U_n \mid \gamma^{(n)} \sim \Gamma^{(i)}\}.$$

Whereas there is great freedom in choosing the elements U_n in $U = U_1 \oplus \cdots \oplus U_k$, the decomposition $U = V^{(1)} \oplus \cdots \oplus V^{(q)}$ is unique up to ordering.

The *characters* of the representation $\Gamma^{(i)}$ are $\chi^{(i)}(g) = \mathrm{tr}[\Gamma^{(i)}(g)]$. These characters are used in projection operators

$$P^{(i)} = \frac{d_i}{|G|} \sum_{g \in G} \chi^{(i)}(g) \alpha_g \tag{4.1}$$

onto the invariant subspaces $V^{(i)} = P^{(i)}(U)$ where d_i is the dimension of the i^{th} irreducible representation. Note that $[\Gamma^{(i)}(g)]$ is a $d_i \times d_i$ matrix.

To proceed we must choose a fixed set of matrix representations $[\Gamma^{(i)}]$ from each equivalence class of irreducible representations. We call these *canonical* matrices. The following calculations are simplified if we make the canonical matrices as simple as possible. It is always possible to choose matrices that are unitary, and we assume that the canonical matrices are unitary.

There is set of projection operators described in [Tinkham, 1964]

$$P_j^{(i)} = \frac{d_i}{|G|} \sum_{g \in G} [\Gamma^{(i)}(g)]_{j,j} \alpha_g, \tag{4.2}$$

where the coefficient of α_g is the j^{th} diagonal element of the matrix $[\Gamma^{(i)}(g)]$. Note that $P^{(i)} = \sum_{j=1}^{d_i} P_j^{(i)}$. The corresponding vector spaces $V_j^{(i)} = P_j^{(i)}(U)$ are not α-invariant, but they are orthogonal, and we shall see that the following decomposition of the representation space is very useful:

$$U = \bigoplus_{i=1}^{q} \left(\bigoplus_{j=1}^{d_i} V_j^{(i)} \right). \tag{4.3}$$

We now consider the effect of the symmetry on commuting linear operators. The theory is much simpler if we assume that the representation space U is complex.

Schur's Lemma. *Suppose Γ_1 and Γ_2 are two irreducible representations of G on $\mathbb{C}^{d_1}$ and $\mathbb{C}^{d_2}$, respectively, and $S : \mathbb{C}^{d_1} \to \mathbb{C}^{d_2}$ is a linear operator such that $S\Gamma_1(g) = \Gamma_2(g)S$ for all $g \in G$. Then $S = 0$ if Γ_1 and Γ_2 are not equivalent, and $S = cI$ for some $c \in \mathbb{C}$ if $\Gamma_1 = \Gamma_2$.*

Note that Schur's Lemma does not address the case where Γ_1 and Γ_2 are different, but equivalent, representations. This case can be addressed by choosing a basis where Γ_1 and Γ_2 are the same, as in the proof of the following corollary. An abstract version of this corollary can be found in [Sagan, 1991, Theorem 1.2.8].

Corollary 4.4. *Suppose that $U = \mathbb{C}^N$ is a representation space for α that is decomposed as in (4.3), and $T : U \to U$ is a linear operator that commutes with α. That is, $\alpha_g T = T\alpha_g$ for all $g \in G$. Then each of the spaces $V_j^{(i)}$ is T-invariant, and the operators $T_j^{(i)} := T|_{V_j^{(i)}}$ decompose T as*

$$T = \bigoplus_{i=1}^{q} \left(\bigoplus_{j=1}^{d_i} T_j^{(i)} \right). \tag{4.5}$$

Furthermore, $T_j^{(i)}$ is similar to $T_{j'}^{(i)}$.

Proof. By complete reducibility, $U = \bigoplus_{n=1}^{k} U_n$, where $\alpha|_{U_n}$ is equivalent to the irreducible representation $\Gamma^{(i_n)}$, with $i_n \in \{1, \ldots, q\}$. We can write T in terms of k^2 blocks $T_{m,n} = P_{U_m} \circ T|_{U_n} : U_n \to U_m$. For each n, we can choose a basis $U_n = \text{span}\{e_{n,j} \mid j = 1, \ldots, d_{i_n}\}$ such that $P_j^{(i)} e_{n,j'} = \delta_{i,i_n} \delta_{j,j'} e_{n,j}$, and $\alpha_g(e_{n,j}) = \sum_{j'=1}^{d_{i_n}} e_{n,j'} [\Gamma^{(i_n)}(g)]_{j',j}$. In other words, the basis vectors $e_{n,j} \in U_n$ transform like the standard basis vectors $e_j \in \mathbb{R}^{d_{i_n}}$ do when multiplied by the matrices $[\Gamma^{(i_n)}(g)]$. If $i_n = i_m$, then $\alpha|_{U_n} = \alpha|_{U_m}$. Thus, Schur's Lemma implies

$$T(e_{n,j}) = \sum_{m=1}^{k} e_{m,j}\, c_{m,n}$$

where $c_{m,n} = 0$ if $i_m \neq i_n$. So, if $i_m = i_n$ then $T(e_{n,j})$ is a sum over $e_{m,j}$ with the same j. The spaces $V_j^{(i)}$ that we defined in terms of projection operators can be written as

$$V_j^{(i)} = \text{span}\{e_{n,j} \mid i_n = i\},$$

and it is now clear that $V_j^{(i)}$ is T-invariant. Finally, $T_j^{(i)}$ is similar to $T_{j'}^{(i')}$ if $i = i'$, since in the basis we have constructed they are represented by the same matrix. □

Remark 4.6. The spectrum of T is the set of eigenvalues of the $k \times k$ matrix C, with elements $c_{m,n}$. The matrix C separates into q diagonal blocks $C^{(i)}$, one for each irreducible representation class of G. If λ is an eigenvalue of $C^{(i)}$, then λ is an eigenvalue of T with multiplicity at least d_i. If the matrix C has any multiple eigenvalues, then we say that T has *accidental degeneracy*. In this case, a perturbation of T that commutes with α can be chosen so that the perturbed C matrix has simple eigenvalues. Barring accidental degeneracy, every eigenvalue of T corresponds to a unique irreducible representation $\Gamma^{(i)}$, the eigenvalue has multiplicity d_i, and an orthonormal set of eigenvectors of this eigenvalue can be chosen, one from each of the d_i subspaces $V_j^{(i)}$, $j \in \{1, 2, \ldots, d_i\}$. These d_i eigenvectors can be used as a basis for one irreducible space U_n. In this way, we can write $U = \bigoplus_{n=1}^{k} U_n$, where each irreducible component U_n is the eigenspace of an eigenvalue λ_n of T.

If we require the spectrum of a linear operator $T : \mathbb{R}^N \to \mathbb{R}^N$ that commutes with a representation on a *real* vector space, we first complexify to the operator $\tilde{T} : \mathbb{C}^N \to \mathbb{C}^N$. The spectra of T and $\tilde{T}$ are the same, so the consequences of Schur's Lemma hold *provided* we consider representations $\Gamma^{(i)}$ which are irreducible over the field $\mathbb{C}$. Sometimes an irreducible representation over $\mathbb{R}$ breaks up into two complex conjugate irreducible representations over $\mathbb{C}$. The eigenvalues of T associated with this pair of representations are complex conjugates. If T is self-adjoint, and thus has real eigenvalues, this causes "accidental degeneracies." For the Laplacian operator on the snowflake domain we do not have to consider this complication since the irreducible representations we need are the same over the field of real or complex numbers.

We now apply the general theory to the eigenvalue equation (1.1). The symmetry group of the snowflake region, as well as the set of grid points in Ω, is the dihedral group

$$\mathbb{D}_6 = \langle \rho, \sigma \mid \rho^6 = \sigma^2 = 1, \rho\sigma = \sigma\rho^5 \rangle.$$

It is convenient to define $\tau = \rho^3\sigma$. Note that $\sigma\tau = \tau\sigma = \rho^3$, and ρ^3 commutes with every element in $\mathbb{D}_6$. The standard action of $\mathbb{D}_6$ on the plane is

$$\begin{aligned} \rho \cdot (x, y) &= \left(\tfrac{1}{2}x + \tfrac{\sqrt{3}}{2}y, -\tfrac{\sqrt{3}}{2}x + \tfrac{1}{2}y\right) \\ \sigma \cdot (x, y) &= (-x, y) \\ \tau \cdot (x, y) &= (x, -y). \end{aligned} \tag{4.7}$$

In this action ρ is a rotation by $60°$, σ is a reflection across the y-axis, and τ is a reflection across the x-axis.

For a given grid with N points in Ω, the $\mathbb{D}_6$ action on the plane (4.7) induces a group action on the integers $\{1, 2, 3, \ldots, N\}$ defined by $x_{g \cdot i} = g \cdot x_i$. There is also a natural action on the space of all functions from Ω to $\mathbb{R}$, $U = \mathbb{R}^N$, defined by $(g \cdot u)(x_i) = u(g^{-1} \cdot x_i)$ for all $u \in U$ and $g \in \mathbb{D}_6$. With the usual identification $u_i = u(x_i)$, this action corresponds to a linear representation α of $\mathbb{D}_6$ on $U = \mathbb{R}^N$ defined by $(\alpha_g(u))_i = u_{g^{-1} \cdot i}$.

There are exactly 6 irreducible representations of $\mathbb{D}_6$ up to equivalence. Our canonical matrices are listed in Table 4. Since we have chosen a set of real matrices, $P^{(i)}$ and $P_j^{(i)}$ are projection operators on both $\mathbb{R}^N$ and $\mathbb{C}^N$. We can write the representation space $U = \mathbb{R}^N$ as

$$U = V^{(1)} \oplus V^{(2)} \oplus V^{(3)} \oplus V^{(4)} \oplus V_1^{(5)} \oplus V_2^{(5)} \oplus V_1^{(6)} \oplus V_2^{(6)},$$

where each of the real vector spaces $V^{(i)}$ and $V_j^{(i)}$ is invariant under any commuting linear operator on U. There are just six spaces in this decomposition regardless of the number of grid points N. On the other hand, the decomposition $U = \sum_{n=1}^{k} U_n$ has thousands of irreducible components U_n when N is large.

In the remainder of this section we use T to refer to the negative Laplacian *operator*. The results of Corollary 4.4 hold, since T commutes with the $\mathbb{D}_6$ action on U. We will use the terms

i	$[\Gamma^{(i)}(\rho)]$	$[\Gamma^{(i)}(\sigma)]$	$[\Gamma^{(i)}(\tau)]$
1	1	1	1
2	1	-1	-1
3	-1	1	-1
4	-1	-1	1
5	$\begin{pmatrix} -1/2 & \sqrt{3}/2 \\ -\sqrt{3}/2 & -1/2 \end{pmatrix}$	$\begin{pmatrix} 1 & 0 \\ 0 & -1 \end{pmatrix}$	$\begin{pmatrix} 1 & 0 \\ 0 & -1 \end{pmatrix}$
6	$\begin{pmatrix} 1/2 & \sqrt{3}/2 \\ -\sqrt{3}/2 & 1/2 \end{pmatrix}$	$\begin{pmatrix} 1 & 0 \\ 0 & -1 \end{pmatrix}$	$\begin{pmatrix} -1 & 0 \\ 0 & 1 \end{pmatrix}$

TABLE 4. A representative from each of the six equivalence classes of irreducible matrix representations of $\mathbb{D}_6$. These canonical matrices are real, but the representations are nevertheless irreducible over the complex numbers. The homomorphism condition $\Gamma^{(i)}(gh) = \Gamma^{(i)}(g)\Gamma^{(i)}(h)$ allows all of the matrices to be computed from $[\Gamma^{(i)}(\rho)]$ and $[\Gamma^{(i)}(\rho)]$. The last column is included for convenience. The representation $\Gamma^{(6)}$ corresponds to the standard action of $\mathbb{D}_6$ on the plane (4.7).

eigenvectors and eigenfunctions of T interchangeably, since the vector $u \in \mathbb{R}^N$ is a function on the N grid points.

The numbering, 1 through 6, of the irreducible representations of $\mathbb{D}_6$ is somewhat arbitrary. Therefore we give the names $V_{p_x p_y d}$ to the 8 T-invariant spaces $V_j^{(i)}$, where p_x and p_y describe the parity of the functions under the reflections σ and τ respectively, and d is the dimension of the associated irreducible representation. Some calculations allow us to give simple descriptions these T-invariant spaces without having to appeal to the projection operators:

$$
\begin{aligned}
V_{++1} := V^{(1)} &= \{u \in U \mid \rho \cdot u = u,\ \sigma \cdot u = u,\ \tau \cdot u = u\} \\
V_{--1} := V^{(2)} &= \{u \in U \mid \rho \cdot u = u,\ \sigma \cdot u = -u,\ \tau \cdot u = -u\} \\
V_{+-1} := V^{(3)} &= \{u \in U \mid \rho \cdot u = -u,\ \sigma \cdot u = u,\ \tau \cdot u = -u\} \\
V_{-+1} := V^{(4)} &= \{u \in U \mid \rho \cdot u = -u,\ \sigma \cdot u = -u,\ \tau \cdot u = u\} \\
V^{(5)} &= \{u \in U \mid \rho^3 \cdot u = u,\ u + \rho^2 \cdot u + \rho^4 \cdot u = 0\} \\
V^{(6)} &= \{u \in U \mid \rho^3 \cdot u = -u,\ u + \rho^2 \cdot u + \rho^4 \cdot u = 0\} \\
V_{++2} := V_1^{(5)} &= \{u \in V^{(5)} \mid \sigma \cdot u = u,\ \tau \cdot u = u\} \\
V_{--2} := V_2^{(5)} &= \{u \in V^{(5)} \mid \sigma \cdot u = -u,\ \tau \cdot u = -u\} \\
V_{+-2} := V_1^{(6)} &= \{u \in V^{(6)} \mid \sigma \cdot u = u,\ \tau \cdot u = -u\} \\
V_{-+2} := V_2^{(6)} &= \{u \in V^{(6)} \mid \sigma \cdot u = -u,\ \tau \cdot u = u\}
\end{aligned}
$$

We can use Corollary 4.4 in two different ways. First, we could construct the numerical approximations to the restricted operators $T_j^{(i)}$ and find the eigenvalues and eigenvectors of the corresponding matrices. This has the advantage that the matrices which represent $T_j^{(i)}$ are smaller than those representing T. In section 2 we described the simple structure of the matrices L, which represent T in the standard basis. We have not attempted to construct the more complicated matrices which represent $T_j^{(i)}$.

We use a second approach. We compute eigenvalues and eigenvectors of the full operator T, and use Corollary 4.4 to classify the eigenvalues according to the corresponding irreducible representation. An eigenvector ψ of T will satisfy $P^{(i)}(\psi) = \psi$ for exactly one i, barring accidental

degeneracy. By computing all the projections, we can determine which irreducible representation is associated with the eigenvector. If the irreducible representation has dimension greater than one, then we can choose an orthonormal set of eigenvectors such that each eigenvector lies in a unique $V_j^{(i)}$ using the projections $P_j^{(i)}$.

For our group $G = \mathbb{D}_6$, we do not have to use the full projection operators $P^{(i)}$ and $P_j^{(i)}$. We only need the four projection operators

$$P_{p_x p_y} = \frac{\alpha_1 + p_x \alpha_\sigma + p_y \alpha_\tau + p_x p_y \alpha_{\rho^3}}{4},$$

where $p_x, p_y \in \{+, -\}$. For example $P_{+-}(u) = (u + \sigma \cdot u - \tau \cdot u - \rho^3 \cdot u)/4$. Note that $P_{p_x p_y}(U) = V_{p_x p_y 1} \oplus V_{p_x p_y 2}$. If ψ is an eigenvector with multiplicity 1 and $P_{p_x p_y}\psi \neq 0$, then $P_{p_x p_y}\psi = \psi$ and $\psi \in V_{p_x p_y 1}$. It is noteworthy that we do not have to check for rotational symmetry. Similarly, if ψ is an eigenvector with multiplicity 2 and $P_{p_x p_y}\psi \neq 0$, then $P_{p_x p_y}\psi \in V_{p_x p_y 2}$.

Here is our algorithm to compute the symmetry of the eigenfunctions of T, and to find eigenvectors in the T-invariant spaces $V_j^{(i)}$. First of all, we know from the computed eigenvalues which are simple and which are double. If an eigenvalue λ is simple, then the corresponding eigenvector ψ satisfies $P_{p_x p_y}\psi = \psi$ for exactly one choice of p_x and p_y, and $\psi \in V_{p_x p_y 1}$. If an eigenvalue λ has multiplicity 2, then each of the 2 orthogonal eigenfunctions returned by ARPACK is replaced with the largest of the four projections $P_{p_x p_y}\psi$. Then, the projected eigenfunctions are normalized. If necessary, the eigenfunctions are reordered so that $\psi \in V_{++2}$ comes before $\psi \in V_{--2}$, and $\psi \in V_{+-2}$ comes before $\psi \in V_{-+2}$. This algorithm assumes that there is no accidental degeneracy. We produced a list of the eigenvalues and symmetry types up to the 300^{th} eigenvalue, confirming that there is no accidental degeneracy.

We now explain why replacing each eigenfunction with the largest projection gives two linearly independent eigenfunctions. Suppose ψ and ϕ are two eigenfunctions with the same eigenvalue. Then either $\psi, \phi \in V^{(5)} = V_{++2} \oplus V_{--2}$ or $\psi, \phi \in V^{(6)} = V_{+-2} \oplus V_{-+2}$. Assume that we are in the first case. The eigenfunctions are orthonormal, so that $||\psi||^2 = ||\phi||^2 = 1$ and the inner product $(\psi, \phi) = 0$. We want to replace ψ and ϕ with normalized eigenfunctions $\psi_{++} \in V_{++2}$ and $\psi_{--} \in V_{--2}$. We can write $\psi = a_\psi \psi_{++} + b_\psi \psi_{--}$ and $\phi = a_\phi \psi_{++} + b_\phi \psi_{--}$, where $||\psi||^2 = a_\psi^2 + b_\psi^2 = 1$, $||\phi||^2 = a_\phi^2 + b_\phi^2 = 1$, and $(\psi, \phi) = a_\psi a_\phi + b_\psi b_\phi = 0$. In other words, $\langle a_\phi, b_\phi \rangle$ and $\langle a_\psi, b_\psi \rangle$ are two orthogonal unit vectors in the a-b plane. Therefore, $a_\psi^2 \geq b_\psi^2$ if and only if $b_\phi^2 \leq a_\phi^2$. Neglecting the numerical coincidence of $a_\psi^2 = b_\psi^2$, this implies that replacing ψ and ϕ by their largest projection will include eigenfunctions of both symmetry types. A similar argument holds for pairs of eigenfunctions in $V_{+-2} \oplus V_{-+2}$.

Figures 6 and 7 shows eigenfunctions with each of the 8 symmetry types for the Dirichlet and Neumann eigenvalue problems, respectively. More eigenfunction contour plots can be found at `http://jan.ucc.nau.edu/~ns46/snow/`.

5. Conclusions.

Table 5 summarizes our best estimates of the eigenvalues, and the symmetry types of the eigenfunctions, for the first few eigenvalues of the linear problem (1.1). We have no error bounds but we can get an indication of the accuracy by comparing our results with those in Banjai's thesis [Banjai, 2003]. Banjai computed the first 20 eigenvalues of the Dirichlet problem, and our eigenvalues agree with his results to four significant figures. This suggests that our results are accurate to four significant figures. Banjai's results for the first ten Dirichlet eigenvalues are more precise.

We are ultimately interested in the connections between the linear problem (1.1) and superlinear elliptic boundary value problems of the form

$$\begin{aligned} \Delta u + f(u) &= 0 \text{ in } \Omega \\ u &= 0 \text{ on } \partial\Omega. \end{aligned} \tag{5.1}$$

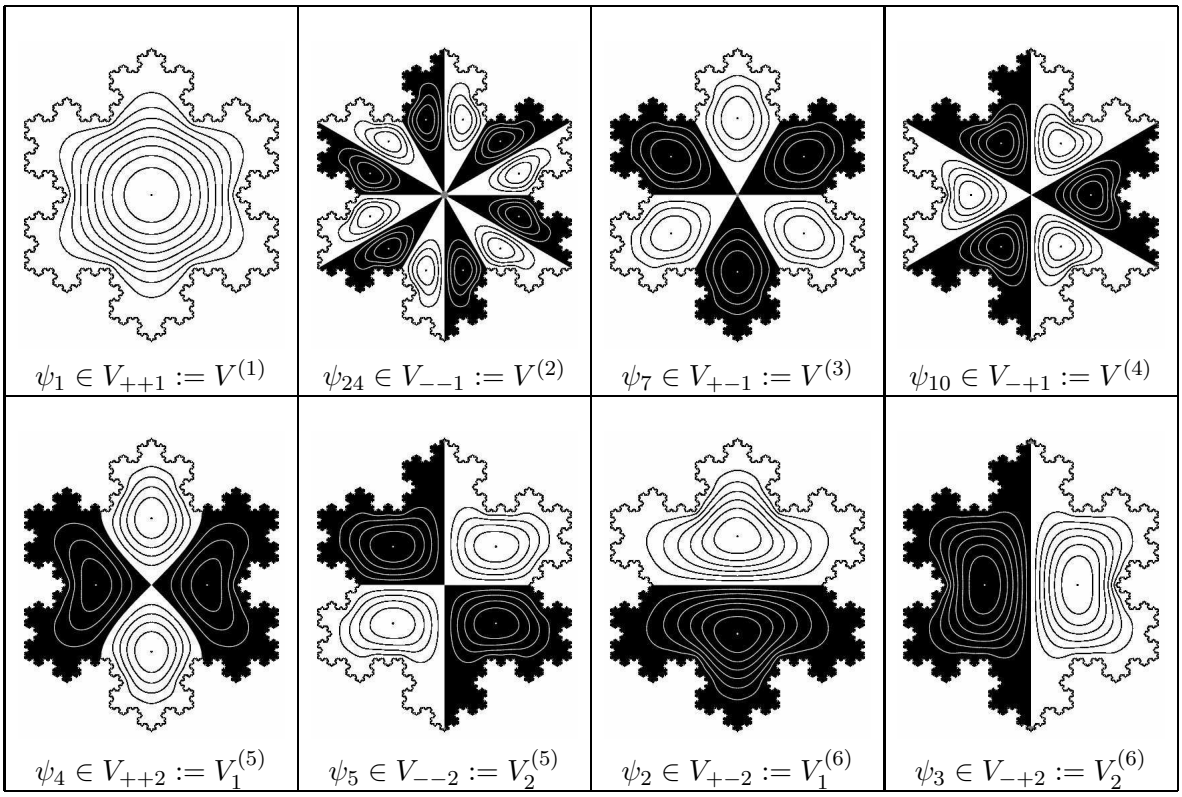

FIGURE 6. The first occurrences of the 8 symmetry types of eigenfunctions of the Laplacian with zero Dirichlet boundary conditions. Each of the eigenfunctions in the first row has a simple eigenvalue. Those in the second row come in pairs. For example, $\lambda_4 = \lambda_5$, since ψ_4 and ψ_5 are each in the invariant subspace $V^{(5)}$ corresponding to the 2-dimensional irreducible representation $\Gamma^{(5)}$. Similarly, $\lambda_2 = \lambda_3$, since ψ_2 and ψ_3 are each in $V^{(6)}$. The eigenfunctions shown respect the canonical decompositions $V^{(5)} = V_1^{(5)} \oplus V_2^{(5)}$ and $V^{(6)} = V_1^{(6)} \oplus V_2^{(6)}$.

The so-called Gradient-Newton-Galerkin-Algorithm (GNGA, see [NS]) seeks approximate solutions $u = \sum_{j=1}^{M} a_j \psi_j^\ell$ to (5.1) by applying Newton's method to the eigenfunction expansion coefficients of the gradient $\nabla J(u)$ of a nonlinear functional J whose critical points are the desired solutions. In [NSS2], we will enumerate the 23 isotropy subgroups of $\mathbb{D}_6 \times \mathbb{Z}_2$, along with the associated fixed point subspaces. These are the possible symmetry types of solutions to (5.1) when f is odd. As a result, we will be able to follow the bifurcation branches of (5.1) by varying the parameter λ in the nonlinearity defined by $f(u) = \lambda u + u^3$. Our symmetry information is crucial to the branch continuation decision making process. In [NSS2] we will find solutions of all 23 symmetry types.

Our catalog of symmetry information is helpful in another way. Given that our basis is chosen in a symmetric fashion and by knowing which invariant subspace a given solution branch's elements lie, it is often possible to know that many of the eigenfunction expansion coefficients are zero. The GNGA requires numerical integration using values at the $N = N_{\mathrm{NSS}}(\ell)$ grid points for each coefficient of the gradient $\nabla J(u)$, as well as for each entry of the Hessian matrix representing $D_2 J(u)$. If we use a basis of eigenfunctions spanning a subspace of dimension M, this amounts to $M^2 + M$ integrations. Using symmetry, we are able to avoid many of these integrations, resulting in a substantial speedup. This becomes very important as we seek high-energy solutions with complex nodal structure, where large values of M and N are required. Each solution is represented by a point on a bifurcation curve, whereby many solutions are sought to complete the branch. Many

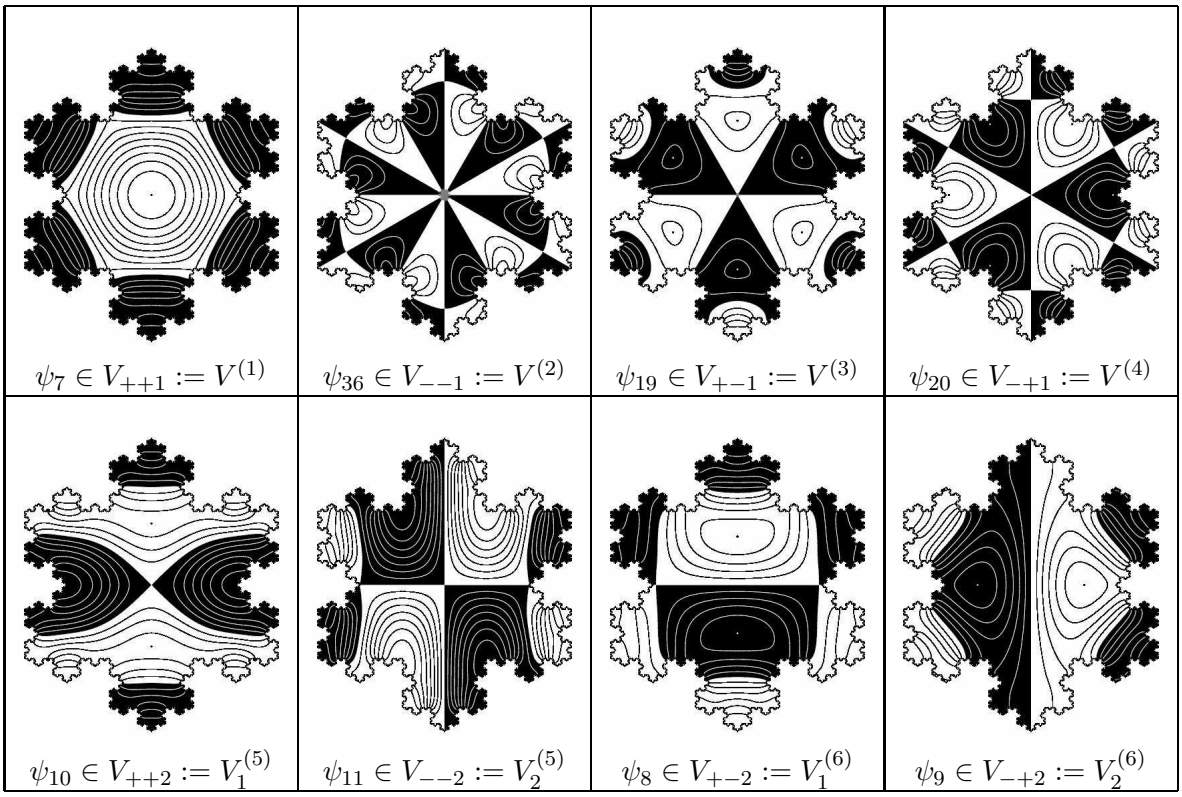

FIGURE 7. The *second* occurrences of the 8 symmetry types of eigenfunctions of the Laplacian, with Neumann boundary conditions. Compare with Figure 6.

of the branches of high-energy solutions have a rich bifurcation structure, resulting in multiple secondary and tertiary branches. There is a substantial time savings obtained by cutting down on the number of required integrations for each Newton step for each solution, on each branch.

In conclusion, this paper presents an efficient, accurate, and easy to implement method for obtaining a basis of eigenfunctions to a subspace which is sufficiently large for performing the eigenfunction expansions required by the GNGA method in solving nonlinear problems of the form (5.1). The major innovations of this work are in the new way we enforce boundary conditions and in the way we are able to choose symmetric representatives of eigenfunctions corresponding to multiple eigenvalues. Our new techniques for generating contour plots are also noteworthy. By further decomposing function space according to symmetry, our nonlinear experiments are much more successful (see [Neuberger, Sieben, and Swift II]). We are currently porting the code to a small cluster using the parallel implementation PARPACK. In the future, we expect to use the techniques of this paper to generate larger numbers of more accurate eigenvalue/eigenfunction approximations, and in so doing, be able to investigate more complicated phenomena and/or problems with regions Ω in $\mathbb{R}^n$, for dimensions $n = 3$ and higher.

REFERENCES

[Banjai & Trefethen, 2003] L. Banjai and L. N. Trefethen, *A Multipole method for Schwarz-Christoffel Mapping of Polygons with Thousands of Sides*, SIAM J. Sci. Comput. **25** vol. 3 (2003), pp 1042–1065.

[Banjai, 2003] L. Banjai, *Computation of Conformal Maps by Fast Multipole Method Accelerated Schwarz-Christoffel Transformation*, Ph.D. Thesis, University of Oxford. (Trinity Term 2003).

[Lapidus, 1991] M. L. Lapidus, *Fractal Drum, Inverse Spectral Problems for Elliptic Operators and a Partial Resolution of the Weyl-Berry Conjecture*, Trans. Anmer. Math. Soc. **325**, pp 465–529.

k	λ_k^{R} (D)	Symmetry	λ_k^{R} (N)	Symmetry
1	39.349	$++1$	0	$++1$
2	97.438	$+-2$	11.842	$+-2$
3	97.438	$-+2$	11.842	$-+2$
4	165.41	$++2$	23.047	$++2$
5	165.41	$--2$	23.047	$--2$
6	190.37	$++1$	27.426	$+-1$
7	208.62	$+-1$	52.210	$++1$
8	272.41	$+-2$	85.552	$+-2$
9	272.41	$-+2$	85.552	$-+2$
10	312.36	$-+1$	112.02	$++2$
11	314.45	$++2$	112.02	$--2$
12	314.45	$--2$	118.34	$-+1$
13	359.53	$++1$	139.38	$+-2$
14	425.40	$+-1$	139.38	$-+2$
15	443.54	$+-2$	139.54	$--1$
16	443.54	$-+2$	147.64	$++1$
17	458.66	$++2$	151.00	$++2$
18	458.66	$--2$	151.00	$--2$
19	560.41	$+-2$	183.64	$+-1$
20	560.41	$-+2$	197.50	$-+1$
21	566.79	$++2$	207.10	$+-2$
22	566.79	$--2$	207.10	$-+2$
23	595.18	$++1$	216.81	$++2$
24	617.70	$--1$	216.81	$--2$

TABLE 5. The first 24 eigenvalues of the negative Laplacian, and the symmetry of the corresponding eigenfunctions, with Dirichlet or Neumann boundary conditions. The Richardson extrapolations for the eigenvalues are given. A comparison with Banjai's thesis suggests that our results are accurate to four significant figures. The symmetry indicates the space containing the eigenfunction. For example, the first eigenfunction is in V_{++1} for both boundary conditions. We follow the convention that V_{++2} is listed before V_{--2}, and V_{+-2} is listed before V_{-+2}.

[Lapidus et al., 1996] M .L. Lapidus, J. W. Neuberger, R. L. Renka, and C. A. Griffith, *Snowflake Harmonics and Computer Graphics: Numerical Computation of Spectra on Fractal Drums*, International Journal Bifurcation and Chaos **6** no. 7 (1996), pp 1185–1210.

[Lapidus and Pang, 1995] M. L. Lapidus and M. M. H. Pang, *Eigenfunctions on the Koch Snowflake Domain*, Commun. Math. Physics **172** no. 2 (1995), pp 359–376.

[Johnson and Riess, 1982] L. Johnson and R. Riess, *Numerical Analysis*, Addison-Wesley : Reading, Mass. (1982).

[Lehoucq et al., 1998] R. B. Lehoucq, D. C. Sorensen, and C. Yang *ARPACK users' guide: Solution of large-scale eigenvalue problems with implicitly restarted Arnoldi methods. Software, Environments, and Tools.* Society for Industrial and Applied Mathematics (SIAM) : Philadelphia, PA. (1998).

[Neuberger and Swift, 2001] John M. Neuberger and James W. Swift *Newton's method and Morse index for semilinear elliptic PDEs* International Journal Bifurcation and Chaos **11** no. 3 (2001), pp 801–820.

[Neuberger, Sieben, and Swift II] John M. Neuberger, Nandor Sieben, and James W. Swift *Symmetry of Solutions to Semilinear Dirichlet Problems on Koch's Snowflake*, preprint, 2003.

[Sagan, 1991] B. E. Sagan *The symmetric group*, Wadsworth & Brooks/Cole Adv. Books Software, Pacific Grove, CA, 1991.

[Scott, 1964] W. R. Scott *Group theory*, Prentice Hall, Englewood Cliffs, N.J., 1964.

[Sternberg, 1994] S. Sternberg, *Group Theory and Physics* Cambridge University Press, Cambridge (1994).

[Tinkham, 1964] M. Tinkham, *Group Theory and Quantum Mechanics* McGraw-Hill Inc., New York (1964).

E-mail address: John.Neuberger@nau.edu, Nandor.Sieben@nau.edu, Jim.Swift@nau.edu

Department of Mathematics and Statistics, Northern Arizona University PO Box 5717, Flagstaff, AZ 86011-5717, USA